Compact OWC Receiver

Compact OWC Receiver: Micro-Lens and PD Array on Glass Interposer

Yuchen Song, Mikolaj Wolny, Chenhui Li, Ketemaw Addis Mekonnen, *Member, IEEE*, Carina Ribeiro Barbio Correa, *Student Member, IEEE*, Marc Spiegelberg, *Member, IEEE*, Eduward Tangdiongga, *Member, IEEE*, and Oded Raz, *Member, IEEE*

***Abstract*—In this article, we propose a compact optical wireless receiver based on micro-lens and photodiode array flip-chipped on a glass interposer. With simulation models and experiments, we verify the performance of two optical wireless communication receivers assembled based on this structure with gigabit and high-speed photodiodes. First, co-integrated gigabit photodiodes and micro-lenses indicate that micro-lenses can deliver a 3.5 dB gain of light collection efficiency to the gigabit photodiode array while keeping the field of view larger than ±18 degrees. Besides, a 5.5 Gbps maximum throughput has been verified by this optical wireless communication receiver with discrete multitone modulation. Moreover, co-integrated high-speed photodiodes and micro-lenses prove that micro-lenses realize a 26.6 dB improvement in light collection efficiency, enabling a 10 Gbps error-free connection using as little as −0.5 dBm transmission power. Those results conclude that the co-integration of micro-lenses on the photodiode array can enhance the light collection efficiency of the photodiode array while keeping a larger field of view, providing a high-performance, low-cost solution for the receiver of optical wireless links.**

***Index Terms*—Optical wireless receiver, micro-lens array, photodiode array, flip chip, glass interposer, light collection efficiency, field of view, discrete multitone modulation.**

I. Introduction

OPTICAL wireless communication (OWC) is emerging as a competitive technological solution for next-generation high-capacity wireless networks due to its abundant unlicensed spectrum [1]. The OWC can meet the booming demand for wireless connectivity for indoor user-based scenarios and high-speed optical interconnects. In indoor user-based scenarios, shown in Fig. 1(a), infra-red beam-steered OWC systems are more energy-efficient since the optical beams are only directed to users asking for a connection [2]. Besides, improved privacy is guaranteed as each user gets its beam, avoiding shared capacity or the ability to eavesdrop. Moreover, benefiting from mature technologies of fiber-optic communication and the broad deployment of passive optical networks, the availability and reliability of the OWC technology can be high, and the deployment cost can be low. Furthermore, for high-speed optical networks, OWC links can potentially optimize the fiber-based systems in data centers and free-space optical (FSO) terrestrial links because of their simplicity in deployment and reconfiguration [3].

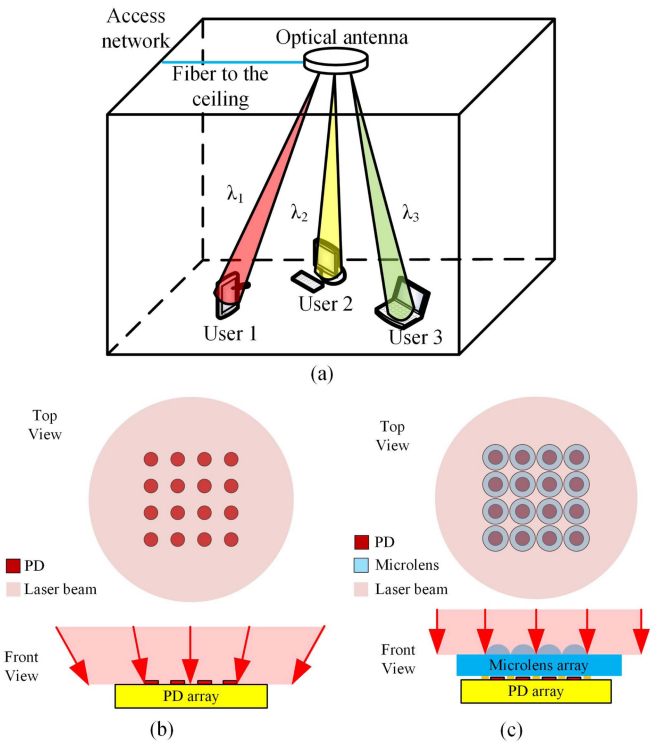

Fig. 1. (a) Indoor wireless scenarios made by fiber to the (ceiling) room and last meters OWC; (b) Optical receiver using PD array only shows a low fill factor; (c) Optical receiver based on co-integration of PD array + micro-lens array shows large fill factor, hence increasing light collection efficiency.

Manuscript received 21 February 2023; revised 21 May 2023; accepted 6 June 2023. Date of publication 13 June 2023; date of current version 2 December 2023. This work was supported in part by the Dutch Organization for Scientific Research (NWO) through the Gravitation Program Grant Center for Integrated Nanophotonics and through Perspectief Program Optical Wireless Superhighways: Free Photons and in part by China Scholarship Council. *(Corresponding authors: Yuchen Song; Chenhui Li.)*

Yuchen Song, Mikolaj Wolny, Carina Ribeiro Barbio Correa, Marc Spiegelberg, Eduward Tangdiongga, and Oded Raz are with the The Electro-Optical Communication System Group, Eindhoven Hendrik Casimir Institute, Eindhoven University of Technology, 5612AP Eindhoven, The Netherlands (e-mail: y.song1@tue.nl; m.wolny@tue.nl; c.ribeiro.barbio.correa@tue.nl; M.Spiegelberg@tue.nl; e.tangdiongga@tue.nl; o.raz@tue.nl).

Ketemaw Addis Mekonnen is with the The TNO Holst Center, 5605KN Eindhoven, The Netherlands (e-mail: ketema.mekonnen@tno.nl).

Chenhui Li is with the The College of Information Science and Electronic Engineering, Zhejiang University, Hangzhou 310027, China, and also with the Research Center for Intelligent Optoelectronic Computing, Zhejiang Lab, Hangzhou, Zhejiang 311121, China (e-mail: Chenhui.Li@zju.edu.cn).

Color versions of one or more figures in this article are available at https://doi.org/10.1109/JLT.2023.3285154.

Digital Object Identifier 10.1109/JLT.2023.3285154

However, working with narrow optical beams faces various technical challenges, including, for example, the blockage of OWC signals by obstacles (also named non-line of sight, NLOS, limitation) [4], [5], [6] and developing high-speed OWC receivers with good alignment tolerance [7], [8]. The challenge we want to address in this article is the limited performance of current OWC receivers on the field of view (FoV) and light collection efficiency. The angular reception and net power illuminating the detection part of an OWC receiver will determine the alignment relaxation, the link budget, and, therefore, the throughput.

The limited performance of current high-speed OWC receivers comes from the nature of the high-speed photodiode (PD) that transforms the optical signals into electrical ones. For PDs operating at high speeds, the capacitance of the PD needs to be small to keep large bandwidth, which translates to a small optical aperture size of the PD that receives little optical power from free space. Avalanche PD (APD) is a possible choice for high-speed OWC receivers thanks to its higher responsivity allowing for signal detection even with a smaller optical aperture [9], [10]. Even so, APDs are more expensive and suffer from additional avalanche noise, which results in a low signal-to-noise ratio (SNR) in OWC scenarios where optical power is low due to eye safety. Besides, standard lenses can be packaged with PDs to increase the light collection efficiency of OWC receivers [11], [12], [13], [14]. Nevertheless, the longer focal lengths of standard lenses restrict the FoV of the optical receiver to a small value. Besides, the alignment and assembly of bulky lenses with diameters of a few millimeters and PD apertures with diameters of tens of micrometers are challenging and expensive. Moreover, integrating PDs into a PD array can offer a larger detection area while maintaining the bandwidth of a single photodiode [7], [8]. However, for electrical pad deposition and cross-talk suppression, spacings between the PDs limited the light collection efficiency of the OWC receiver composed of the PD array, shown in Fig. 1(b).

Micro-lenses potentially offer a better solution as an optical element coupling light from free space to the sensitive area of a high-speed PD. With smaller focal lengths and aberrations, micro-lenses can focus light to tiny points while providing a larger FoV. Besides, the alignment of PDs and micro-lenses is more practical since their sizes are of the same order of magnitude. Moreover, the assembled receiver can be compact by integrating PDs and micro-lenses into one substrate. However, micro-lenses still offer a limited aperture that collects small amounts of light power from free space. Therefore, we proposed that combining the discrete PD array and the micro-lens array can offer OWC receivers high light collection efficiency and large FoV as in [15]. However, as a theoretical study using the micro-lens array as a light coupling structure, the previous study based on discrete elements showed limited gain improvement (1 dB) from micro-lenses offering larger FoV and higher cost on the packaging.

In this work, we study the PD + micro-lens structure in detail by presenting a compact, low-cost OWC receiver with the PD array and micro-lens array integrated on a single glass interposer, as shown in Fig. 1(c), enhancing the light-collection efficiency while keeping a larger FoV. With this new assembly, first, we omit the through silicon vias (TSVs) that avoid Fresnel reflections using a single glass interposer. Second, thanks to the spherical side of the micro-lens facing the laser beam, we avoid the total internal reflection on the spherical surface with a smaller RoC [15]. Third, we explore more advanced modulation formats than on-off keying, including PAM4 and discrete multitone (DMT), on this new assembly, leveraging the bandwidth of PDs and trans-impedance amplifiers (TIAs) to achieve higher throughput. Fourth, we study the scalability of this structure in speed, arrangement, and efficiency by replacing the 4×4 Gigabit Ethernet (GbE) PD array with a high-speed hexagonal (2 + 3 + 2) PD array integrated with larger micro-lenses. We prove a larger gain of light collection efficiency from a micro-lens array that enables high-speed data transmission with this high-speed OWC receiver. This article is organized into four sections. Section II details the receiver design and simulation, which reveals the structure of this OWC receiver and the simulation results of the optical system and electrical circuits. Section III gives the main results from experimental verification of the design, showing the processes of sample fabrication, experiment system setup, and experiment results. Section IV presents conclusions.

II. OWC Receiver Design and Simulation

The schematic of the suggested arrangement of PDs, micro-lenses, and the interposer is shown in Fig. 1(c). Several parameters define the performance of the OWC receiver composed of the micro-lens array + PD array: the diameter of the micro-lenses, RoC of the micro-lens, apertures of PDs, and the thickness of the glass wafer. In this article, our discussion focuses on standard, commercially available PDs manufactured with a typical size of 250 μm $\times$ 250 μm, which offer the lowest cost for developing this technology.

As a light collection element, the micro-lens array improves the light collection efficiency of the PD array by fill factor (the ratio of the light-sensitive area of an optical receiver to the total area of an optical receiver [16]) recovery. Besides, the gain of light collection efficiency from micro-lens increases when the PD aperture decreases, maintaining a fixed light collection efficiency depending on the micro-lens array, no matter how small the PD aperture is, unless reaching the diffraction limit. The relationship between the gain from micro-lenses with a diameter of 250 μm versus the PD aperture is shown in Fig. 2(a). We can see that for a PD array consisting of PDs with an aperture of 25 μm and 150 μm in diameter, the gain from the micro-lens is 20 dB and 4.4 dB, respectively.

Besides, as a lens-based structure, the FoV of the OWC receiver composed of the micro-lens + PD array also follows the law of conservation of etendue, as shown in Fig. 2(b), calculated with photoresist micro-lens. However, the micro-lenses offer much smaller focal lengths than standard lenses, especially for high refractive-index micro-lenses, so they maintain a larger FoV than the standard lenses. For photoresist micro-lens with a diameter of 250 μm (RoC $>$125 μm), designed for 250 μm PD-PD spacing, the maximum theoretical FoV is $\pm$18.3 degrees for 1 GHz PDs with an aperture of 150 μm and $\pm$3.1 degrees

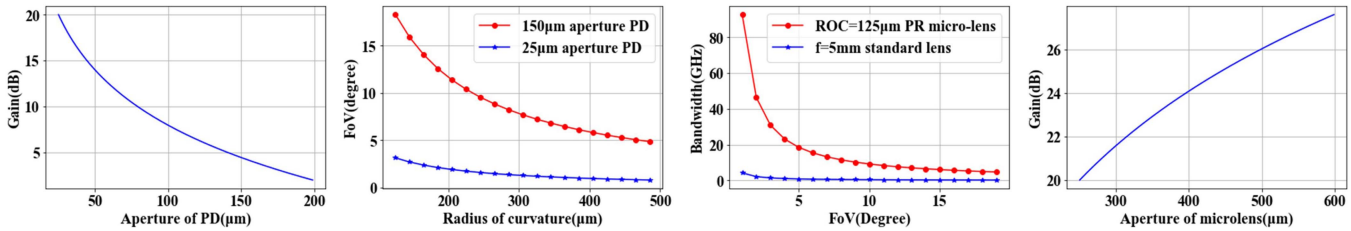

Fig. 2. (a) Gain from micro-lens with 250 μm aperture versus aperture of PD; (b) FoV versus RoC of micro-lens; (c) Bandwidth of OWC receiver versus FoV; (d) Gain from micro-lens to PDs of 25 μm aperture versus aperture of the micro-lens.

for 25 GHz PDs with an aperture of 25 μm. The conservation of etendue also leads to a trade-off between FoV and the receiver's bandwidth (denoted by B) and, therefore, the system's bandwidth. This trade-off can be expressed with (1) [17] and (2) where ε_0 is the permittivity of vacuum, ε_r is the relative permittivity of the PD substrate, R_L is the load resistance, v_s is the carrier saturation velocity, f is the focal length of micro-lenses, and D_{PD} is the diameter of the PD aperture. The FoV is inversely proportional to the bandwidth of the OWC receiver (thus the bandwidth of the system) as shown in Fig. 2(c), taking InP-based PD ($\epsilon_r = 12.4, v_s = 2.6 \times 10^7$ cm/s) with R_L of 50 Ω as an example, but micro-lens with smaller focal length offers larger margin than the standard lens.

$$B = \frac{1}{\pi D_{PD} \sqrt{\frac{\varepsilon_0 \varepsilon_r R_L}{0.44 v_s}}} \tag{1}$$

$$FoV = \arctan\left(\frac{D_{PD}}{2f}\right) \tag{2}$$

Moreover, in some use cases of high-speed OWC links, the transmitters and receivers are fixed once deployed, so a small FoV is acceptable. In those cases, micro-lenses with extended sizes (with smaller minimum focal lengths) can be applied to capture more light from free space and increase the gain of light collection efficiency from the micro-lenses. Fig. 2(d) presents the relationship of gain to PDs with an aperture of 25 μm versus diameters of micro-lenses, proving that micro-lenses with a diameter of 600 μm can provide 27.6 dB gain to a high-speed OWC receiver, 7.6 dB higher than the micro-lens with a diameter of 250 μm.

Furthermore, a hexagonal micro-lens array can realize a higher fill factor because the hexagonal micro-lens array is better aligned with the circular beam shape and minimizes the gaps between circular micro-lenses. For example, from the 2×2 micro-lens array to the $2 + 3 + 2$ hexagonal micro-lens array, the fill factor is improved from 68.6% to 77.8%.

In this article, we build up two OWC receivers with around 1.8 mm aperture on glass interposers to verify our design. One based on the previous 4×4 GbE PD array introduced in reference [15], and one based on a currently designed high-speed OWC receiver with $2 + 3 + 2$ hexagonal PD array that has larger bandwidth but small PD aperture (25 μm). The 4×4 GbE PD + micro-lens array is designed to operate in a narrow beam-based indoor OWC system (up to 2 m with 3.5 mm beam diameter) with the beam steering [18] and user localization scheme offering <3-millimeter tolerance within 2 m distance [19]. The $2 + 3 + 2$ hexagonal PD array is designed to operate in narrow-beam (3 mm) short-range (1 m-3 m) data center wireless links, with a tracking and pointing system to maintain optimal throughput [20]. The OWC receiver can be further optimized by putting more PD + micro-lens cells in the array to increase its aperture, which offers larger transmitter-receiver alignment tolerance and, thus, enable an OWC link with a more extended range.

Below we detailed the result of optical simulation using ZEMAX that takes aberration into account to simulate the performance of those two OWC receivers. Further, to complement the optical simulation, we include the simulation results using the Advanced Design System (ADS) to study the influence of the electrical circuit design on the performance of the OWC receiver.

A. *Optical Simulation*

For the optical simulation of the GbE OWC receiver using the previous mask design and test link [15], we build a similar model as the previous one using ZEMAX to estimate the performance of the compact OWC receiver. The RoC of the micro-lens is 127 μm, arranged like the inset of Fig. 3(b), and aligned with the PD array. The thickness of the glass interposer is 200 μm, matching the focal length of micro-lenses. Fig. 3(a) and (b) show the simulation results, which indicates that the improvement of the light collection efficiency from integrating photoresist micro-lens array on PD array is 3.8 dB, with a tolerance improvement from $\pm$1.1 mm to $\pm$1.5 mm when taking -17.0 dBm as the threshold for error-free connection [15]. Besides, the FoV of this structure is more than $\pm 20^\circ$ while the GbE PDs have an aperture of 150 μm. The simulation results also show that co-integrating the PDs and micro-lenses on a single glass interposer avoids the total internal reflection that limits the gain as experienced in our previous report [15].

We also test the performance of the hexagonal $(2 + 3 + 2)$ PD + micro-lens array model in the same OWC simulation link built up in ZEMAX. The PDs have an aperture of 25 μm, ensuring their high-speed performance. The micro-lenses have a diameter of 580 μm and a RoC of 450 μm, arranged in a $2 + 3 + 2$ hexagonal array that covers a Φ1.8 mm circular area and aligned with the PD array, shown in the inset of Fig. 3(d). The thickness of the glass interposer is 1 mm, matching the focal length of

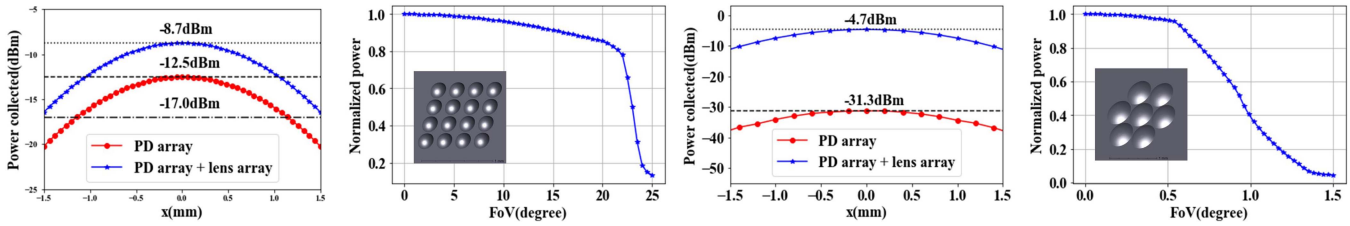

(a) (b) (c) (d)

Fig. 3. (a) Position tolerance of GbE OWC system with and without RoC=127 μm micro-lenses; (b) Normalized optical power from GbE OWC receiver with RoC=127 μm micro-lens arrays versus FoV, inset: the simulation model of 4 $\times$ 4 micro-lens array; (c) Position tolerance of high-speed OWC system with and without RoC=450 μm micro-lenses; (d) Normalized optical power from high-speed OWC receiver with RoC=450 μm micro-lens arrays versus FoV, inset: the simulation model of the hexagonal micro-lens array.

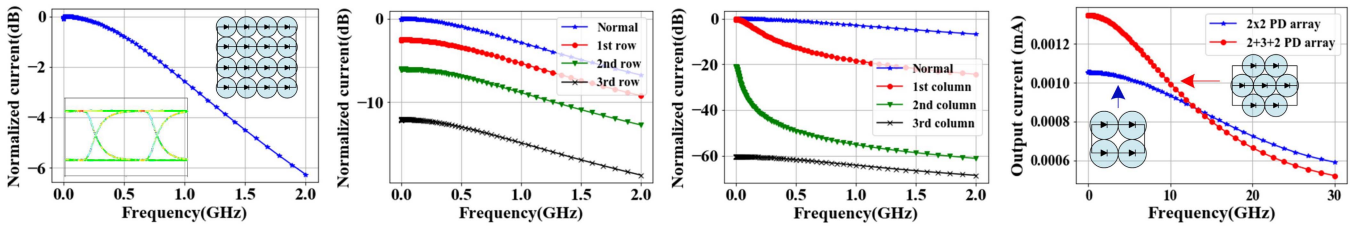

(a) (b) (c) (d)

Fig. 4. (a) Normalized output frequency response, inset: 4 $\times$ 4 PD array setup and eye diagram of 1 Gbps data transmission; (b) Normalized output frequency response while PDs connected in series are blocked; (c) Normalized output frequency response while PDs connected in parallel are blocked; (d) Output frequency response for 2 + 3 + 2 hexagonal PD array arrangement and 2 $\times$ 2 PD array arrangement, inset: 2 $\times$ 2 PD array setup and hexagonal PD array setup.

micro-lenses. Fig. 3(c) and (d) display the simulation results, proving that the hexagonal micro-lens array (2 + 3 + 2) provides 26.6 dB gain of light collection efficiency to the PD array, which comes from the fill factor improved from 0.14% to 77.8%; and the FoV of this OWC receiver is $\pm$0.93 degrees. Considering applications of high-speed OWC receivers, for example, data center OWC links [12] and terrestrial FSO links [21], even such small FoV is acceptable since they are fixed after deployment. Hence the FoV of this modeled OWC receiver is already large enough to handle the challenges in some of those cases [20].

B. *Electrical Design and Simulation*

The bandwidth and electrical gain of the OWC receiver composed of a PD array are analyzed with the mathematical model previously presented in [7]. In this article, in addition to the analytical results shown in our previous reports, we build up a model in ADS to quantify the high-speed performance of the PD array circuit. The model of the PD consists of a signal-dependent current source, a shunt resistor, and a voltage-dependent capacitor.

Firstly, we build the model of the 4 $\times$ 4 GbE PD array model in ADS. The PDs are connected with the 60 μm strip-lines on the glass substrate. The electrical performance of the PD array is evaluated by studying the output current amplitude versus frequency (frequency response) and the eye diagram. The results are shown in Fig. 4(a), indicating the bandwidth of a 4 $\times$ 4 PD array with 260 μm PD-PD spacing is approximately 1.1 GHz. Also, the eye diagram of 1 Gbps sequence transmission is wide open and clean, proving it can handle 1 Gbps data rate transmission.

Besides, we evaluate the influence of non-uniform illumination on the PD array in the simulation model as a detailed verification of the previous analytical model [7], [22]. In this simulation, the signal applied on PDs is canceled row by row (PDs in one row are connected in series) and column by column (PDs in one column are connected in parallel), which mimics blocking the light from the direction of the parallel connection and series connection. The simulation results are shown in Figs. 4(b) and (c), which show that when partial illumination of the PD array takes place, and the beam profile is uneven from the direction of PDs connected in series, the performance of the PD array deteriorates both on signal amplitude and bandwidth. Nevertheless, we do not see this trend when the beam profile is uneven in the parallel direction. The reason for this anisotropy phenomenon is that PDs connected in series flow the same current. Because the blocked PDs generate a small current, have high resistance, and take most of the bias voltage (seized from other PDs in the same row), they will lock the current output and limit the overall bandwidth of the row. Unlike PDs connected in series, PDs connected in parallel are not locked by the same current and thus do not suffer from such a limitation. Therefore, homogenizing beam profile along the PDs connected in series is essential for ensuring the optimum PD array performance. Alternatively, we can add shunt resistors in the PD array for bias voltage homogenization [22]. In our test, we use the transmitter

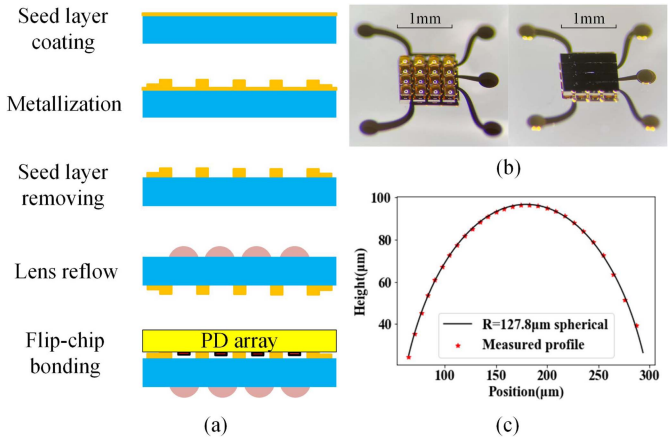

Fig. 5. (a) Process flow of sample fabrication; (b) The assembled PD array (right) with micro-lens array (left); (c) Profile of the reflowed micro-lens.

whose output beam size (3 mm diameter at $1/e^2$ power) is larger than the aperture of the OWC receiver (1.6 mm in diameter for GbE OWC receiver, 1.8 mm in diameter for high-speed OWC receiver). In that case, the light is almost illuminated uniformly on the PD array.

Moreover, we simulate the electrical performance of the high-speed OWC receiver with the PD model having a smaller capacitance. The PDs are connected with the 50 Ω coplanar waveguide (CPW). They are arranged in a hexagonal (2 + 3 + 2, as shown in the inset of Fig. 4(d)) array. Fig. 4(d) shows the output frequency response. The same plot draws the simulation results from the electrical model of 2 × 2 high-speed PD array (as shown in the inset of Fig. 4(d)) in contrast to the hexagonal PD array. Those two arrangements are designed to fit the same circular area. The results indicate that: although the hexagonal PD array has a smaller bandwidth than the M×M PD array because of its higher capacitance, it can offer higher output than the M×M PD array because of its smaller fill factor and higher electrical gain. Considering that the maximum power in the OWC link is limited and the power budget for the free-space OWC link is usually high, the hexagonal PD array supporting data detection with lower optical power will be a better option. So we adopt the hexagonal PD array in our high-speed OWC receiver.

III. Fabrication, Experiment Setup, and Results

In the experiment, we first fabricate and package the samples modeled in the simulation. Then we test the samples in the OWC links.

A. Fabrication Process

The fabrication process of the interposer is illustrated in Fig. 5(a), based on which we introduce the main steps as follows. The glass wafer is made of fused silica wafer, and its refractive index (n = 1.44) is close to photoresist micro-lens (n = 1.55), ensuring a small Fresnel reflection. First, on the front side of the glass wafer, a seed layer of Ti/Au 10 nm/100 nm for electroplating is deposited with the evaporation coating. Second, metalization of 2 μm thick traces and 5 μm thick pads is done on the seed layer according to patterns defined with contact lithography. Third, the seed layer is wet etched to the wafer by KCN and Ti etching solution. Fourth, photoresist AZ 40XT cylinders for lens reflow are developed on the back side of the wafer, then reflowed (140 °C for 60 seconds) to form micro-lenses. In the reflow process, to accurately get the RoC of photoresist micro-lenses designed for the OWC receiver, we apply HMDS treatment on the cleaned glass wafer before the photoresist is spin coated on the glass surface to minimize the change of the photoresist pattern before and after reflow. Fifth, hard baking (300 °C, 30 min) in the vacuum oven is used to stabilize the chemical and thermal proprieties of micro-lenses [23] so that they can go through the high-temperature bonding process during assembly. The profile of the baked micro-lens is shown in Fig. 5(c), indicating a spherical surface with an RoC of 127.8 μm is achieved. Sixth, the wafer is diced into 1 cm×1 cm interposers, which are easy to handle and package with photonic chips. Finally, the PD array (4 pieces of 1 × 4 1.8 GHz bandwidth PD arrays, from Albis Optoelectronics) is flip-chipped on the front side of the interposer, forming the OWC receiver ready for the test, which is shown in Fig. 5(b).

B. Experimental Evaluation in GbE OWC Link

We wire bond the OWC receiver into a PCB-based platform with 10 kΩ trans-impedance amplifier (TIA, HMC799LP3E from Analog Devices) and put it into the OWC link built previously in [15] to test the performance of the GbE OWC receiver, as shown in Fig. 6(a). 1 Gbps $2^{23}-1$ pseudo-random binary sequences, non-return to zero, on-off keying (PRBS23, NRZ, OOK) pattern is used for the test, and the bias voltage for the PD array is set to 0 V.

Firstly, we test the relationship between the transmitter power versus the BER for 1 Gbps data transmission at the 0-degree FoV to see the improvement of light collection efficiency from co-integrating the PD array and micro-lens array on the glass interposer. The results are shown in Fig. 6(b). Comparing results from this OWC receiver to the results of the PD array without micro-lens from reference [15], a 3.5 dB improvement of light collection efficiency is verified. Besides, we study the gain of alignment tolerance between the OWC receiver and transmitter for 1 Gbps data transmission by measuring BER versus transmitter-receiver misalignment under 0 dBm transmitter power. The results, plotted in Fig. 6(c), show that positioning tolerance for error-free data transmission is improved from ±1.1 mm to ±1.5 mm.

Moreover, we characterize the FoV of the OWC receiver by measuring the BER of 1 Gbps data transmission with -8 dBm transmitter power under different illumination angles. The results are shown in Fig. 6(d), which can conclude that the FoV of this OWC receiver is >18 degrees (half angle). Furthermore, we measure the performance of the PD array under partial illumination by partially blocking the PDs from the transmitter with 0 dBm power, copying the process that is done on the simulation model to acquire Fig. 4(b) and (c). The results are

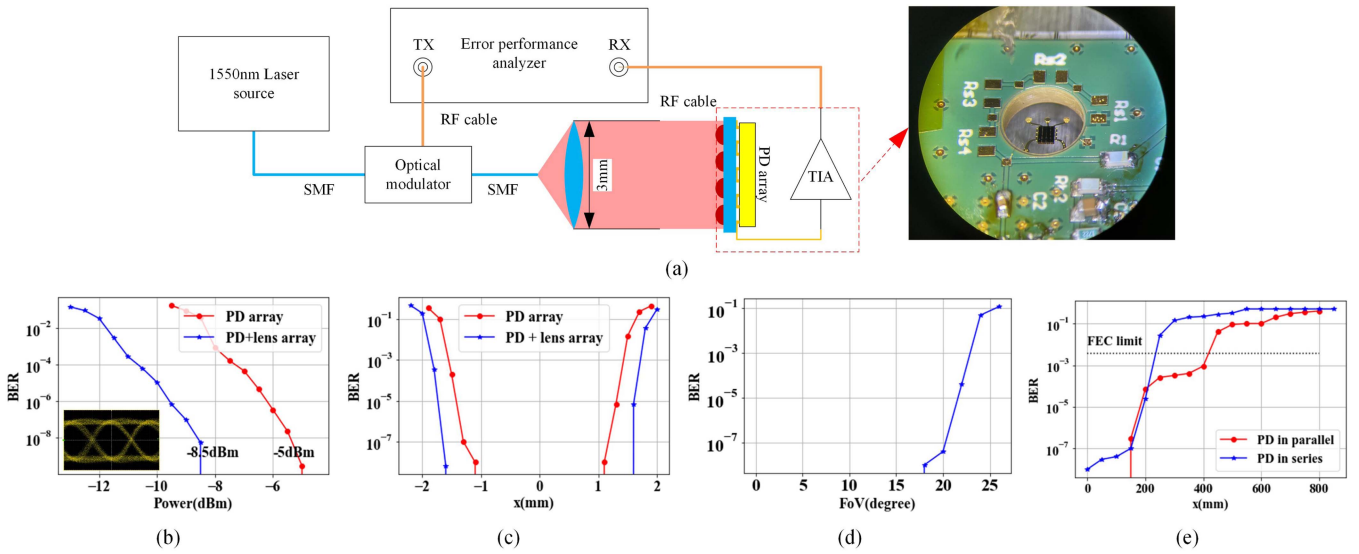

Fig. 6. (a) Experimental setup; (b) BER versus transmitter power for PD array with and without micro-lenses, inset: eye diagram of 1 Gbps signal; (c) BER versus transmitter-receiver misalignment (transmitter power: 0 dBm); (d) BER versus FoV (transmitter power: −8 dBm); (e) BER of the OWC link with partial illumination on the OWC receiver, x-axis: position of card blocking the light along PDs connected in series (blue line) and parallel (red line).

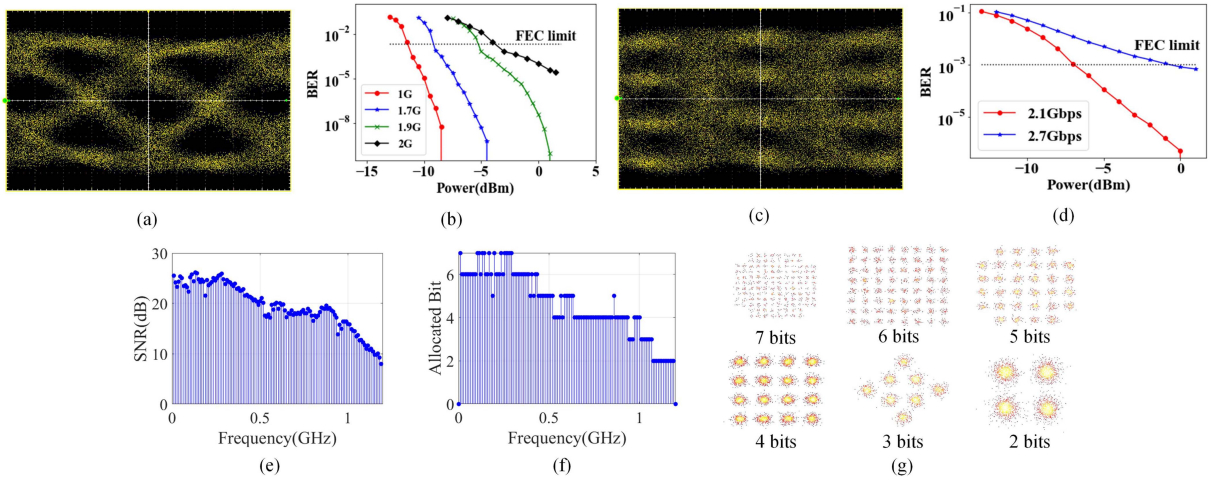

Fig. 7. (a) Eye diagram of 1.9 Gbps signal from the OWC receiver; (b) BER versus transmitter power for OOK signals with 1 Gbps, 1.7 Gbps, 1.9 Gbps, and 2 Gbps data rate; (c) Eye diagram of 2.1 Gbps PAM4 signal from the OWC receiver; (d) BER versus transmitter power for PAM4 signals with 2.1 Gbps, and 2.7 Gbps data rate; (e) Signal-to-noise ratio (SNR) versus frequency for 5.5 Gbps DMT signal detected by OWC receiver; (f) Allocated bit versus frequency for 5.5 Gbps DMT signal detected by OWC receiver; (g) Constellations diagram for each QAM modulation for 5.5 Gbps DMT signal detected by OWC receiver.

in Fig. 6(e), which confirm the more strict requirement of the homogeneity of the beam profile along the direction of the PD array connected in series, consistent with the simulation results.

Apart from the test at the 1 Gbps data rate, we study the performance of this OWC receiver at higher data rates. BER versus transmitter power curves for PRBS23 NRZ OOK patterns with 1.7 Gbps, 1.9 Gbps, and 2.0 Gbps data rates are measured at 0-degree FoV, with 15 V bias voltage on the PD array. The results prove 1.9 Gbps error-free (BER$<10^{-9}$) and 2 Gbps under forward error correction limit (FEC limit, BER$<3.8\times10^{-3}$) data transmission with this receiver, as shown in the Fig. 7(a) and (b). Besides, we test PAM4 data transmission with this OWC receiver. Results, shown in Fig. 7(c) and 7(d), prove the

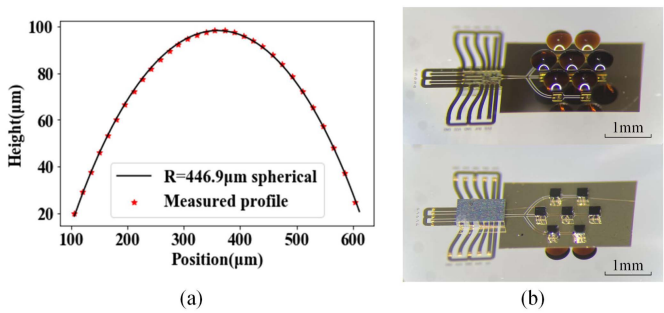

Fig. 8. (a) Profile of reflowed micro-lens for high-speed OWC receiver; (b) The assembled PD array and TIA (down) with micro-lens array (up).

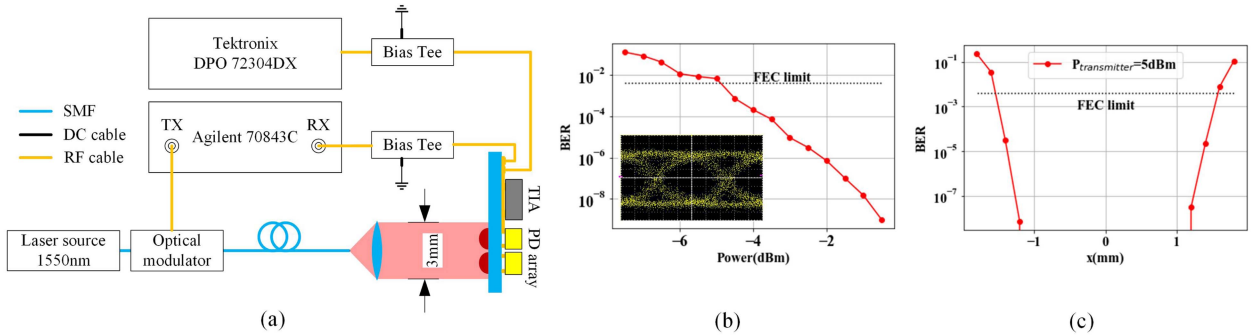

Fig. 9. (a) Experimental setup of 10 Gbps OWC link over 30 cm; (b) BER versus transmitter power for OOK signals with 10 Gbps data rate, inset: eye diagram of the received signal; (c) BER versus transmitter-receiver misalignment (transmitter power: 5 dBm).

2.1 Gbps error-free and 2.7 Gbps under FEC limit PAM4 data transmission with this receiver.

Further, we apply DMT modulation in this OWC test link to make use of most of the bandwidth of the OWC receiver for higher spectral efficiency and, therefore, higher throughputs. The experimental setup of DMT modulation is similar to that shown in Fig. 6(a). The error performance analyzer is replaced with the DMT transmitter (TX) and receiver (RX). TX is a laptop-controlled arbitrary waveform generator (AWG, AWG7122B from Tektronix) that works as a digital-to-analog converter (DAC). It feeds the DMT signal (coded by Matlab) to the optical modulator. RX is a laptop-controlled digital phosphor oscilloscope (DPO, DPO72304DX from Tektronix) that works as an analog-to-digital converter (ADC). It converts the signal from the OWC receiver to digital data analyzed by a laptop. In this article, we create the DMT signal according to the algorithm used in reference [24]. The DMT signal has 128 sub-carriers, evenly distributed from 0 to 1.2 GHz and modulated with quadrature amplitude modulation (QAM). The OWC receiver's ability to recover the data from this DMT signal is studied by measuring the maximum throughput with the BER under the FEC limit.

During the test, we tune the settings for the DMT algorithm to maximize the throughput. Firstly, clipping the DMT signal can relieve the problem of a high peak-to-average power ratio (PAPR). However, clipping deteriorates information, thus limiting the maximum throughput with the BER under the FEC limit. During the test of this OWC receiver, the optimum crest factor (defined in reference [24]) was set to 23 dB for the maximum throughput, indicating a little impact from the PAPR of DMT signal on the OWC link. Besides, the cyclic prefix is used to combat the inter-symbol interference (ISI) in a multipath channel [25]. We apply the optimum cyclic prefix, which is 2% the length of the symbol, to increase the robustness of the detection of the signal and, in combination with the DPO sampling rate at 100 GSa/s, to maximize the throughput.

With the optimized settings, we conclude that the maximum throughput of the OWC link based on this OWC receiver is 5.5 Gbps under the FEC limit. Figs. 7(e) and (f) shows the SNR and allocated bits for each sub-carrier of 5.5 Gbps DMT signal transmission, and Fig. 7(g) shows the constellation diagrams of 5.5 Gbps DMT signal transmission. According to Fig. 7(e), the SNR of the OWC receiver drops below 20 dB for subcarriers with frequencies >700 MHz. Considering that the TIA enables a bandwidth of 700 MHz, closer to the 700 MHz limit than that of PD (1.8 GHz), we can conclude that TIA is the main reason that limits the throughput of this OWC receiver. Adopting TIAs with larger bandwidths can further improve the throughput of this OWC receiver.

C. Experimental Verification With High-Speed OWC Link

As obtained in the simulation section, for a high-speed PD array with a smaller PD aperture, the gain of light collection efficiency from micro-lens is much higher since it significantly expands the area of light that can couple onto the PD array. Therefore, in this second experiment, we assemble a high-speed version of the OWC receiver composed of the micro-lens array and PD array to estimate the feasibility of this design for data transmission with a higher data rate.

The fabrication process of the OWC receiver composed of a high-speed PD + micro-lens array is the same as that of the GbE OWC receiver shown in Fig 5, except for a few modifications in mask design and micro-lens fabrication. First, in the new mask design, the PDs and micro-lenses, with a diameter of 580 μm, are arranged in a hexagonal array $(2+3+2)$ to improve the light collection efficiency of the high-speed OWC receiver where the power budget is high. Second, PDs are connected via 50 Ω CPWs for better high-speed performance. Third, the spin-coating step in the lens reflow process is modified to achieve micro-lens with an RoC of 450 μm. The micro-lens profile achieved is shown in Fig. 8(a), which is a spherical surface with an RoC of 447 μm. According to the calculation with the simulation model, this 3 μm deviation cause only 0.6 dB loss.

The PDs used in high-speed OWC receivers are high-speed commercial PDs (Vertical Integrated Systems, VIS) having an optical aperture of 25 μm and 3 dB bandwidth of 30 GHz (at 5 V bias voltage). The chip size of the PD is 250 μm $\times$ 250 μm, and the fill factor is 0.8% (size of optical aperture divided by the size of the chip). Unlike the GbE OWC receiver where TIA is not integrated with the PD array, the 5.8 kΩ TIA (T56-250 C from the VIS) is flip-chipped closely with the PD array on the same glass interposer to minimize the loss. The assembled $2+3+2$ PD array with TIAs is shown in Fig. 8(b).

We test the high-speed OWC receiver at 10 Gbps OWC link shown in Fig. 9(a). The signal from the transmitter is the 1550 nm laser beam carrying the 10 Gbps PRBS7 NRZ OOK sequence, which transmits through a 0.3 m free space and is received by the high-speed OWC receiver. Then, the signal is converted into an electrical current, amplified by the TIA, and sent to the error analyzer to evaluate the BER of the transmission. Fig. 9(b) shows the relationship between BER and the optical power from the transmitter and the eye diagram of the 10 Gbps signal from the single-ended output of TIA. The results prove 10 Gbps error-free data transmission of this assembled OWC receiver with as little as −0.5 dBm (−4.5 dBm under FEC limit) power from the transmitter. Also, BER versus transmitter-receiver misalignment is measured for the 10 Gbps OWC link with a transmitter power of 5 dBm. As a result, the positioning tolerance of error-free connection for this OWC link is ±1 mm (±1.5 mm under FEC limit).

IV. Conclusion

In this article, we propose a compact OWC receiver by co-integrating PD arrays and micro-lens arrays on a glass interposer.

Firstly, a GbE OWC receiver is designed, fabricated, and tested, showing an improvement of light collection efficiency from photoresist micro-lens of up to 3.5 dB, and the tolerance of the transmitter-receiver misalignment enlarged from ±1.1 mm to ±1.5 mm for a 1 Gbps error-free OWC data transmission. Besides, the FoV of 1 Gbps OWC receiver is kept at ±18 degrees with 150 μm aperture photodiode using photoresist micro-lenses. Finally, the enhanced light collection efficiency allows the OWC receiver to reach higher throughput than 1 Gbps, and 5.5 Gbps maximum throughput is verified with DMT modulation, limited by 700 MHz bandwidth TIA.

Secondly, we use the same integration concept to fabricate a OWC receiver consisting of PDs with higher bandwidth to study its scalability to high speed. With the gain from the micro-lenses, an OWC receiver with an aperture of 1.8 mm is demonstrated, and a 10 Gbps error-free connection has been realized with as little as −0.5 dBm power (−4.5 dBm under FEC limit). Moreover, the transmitter-receiver alignment tolerance of this link is ±1.5 mm (under the FEC limit).

We conclude from the simulation and experimental results that the OWC receiver combining the micro-lens array and the PD array can achieve good light collection efficiency and keep a larger FoV. It is a promising solution for the coupling strategy of small-form and high-speed OWC receivers.

References

[1] Y. Wu et al., *6G Mobile Wireless Networks*. Berlin, Germany: Springer, 2021.

[2] T. Koonen, K. A. Mekonnen, Z. Cao, F. Huijskens, N. Q. Pham, and E. Tangdiongga, "Beam-steered optical wireless communication for industry 4.0," *IEEE J. Sel. Topics Quantum Electron.*, vol. 27, no. 6, Nov./Dec. 2021, Art. no. 6000510.

[3] A. S. Hamza, J. S. Deogun, and D. R. Alexander, "Wireless communication in data centers: A survey," *IEEE Commun. surveys Tuts.*, vol. 18, no. 3, pp. 1572–1595, thirdquarter 2016.

[4] S. Jovkova and M. Kavehard, "Multispot diffusing configuration for wireless infrared access," *IEEE Trans. Commun.*, vol. 48, no. 6, pp. 970–978, Jun. 2000.

[5] P. W. Berenguer et al., "Optical wireless MIMO experiments in an industrial environment," *IEEE J. Sel. Areas Commun.*, vol. 36, no. 1, pp. 185–193, Jan. 2018.

[6] Z. Cao, X. Zhang, G. Osnabrugge, J. Li, I. M. Vellekoop, and A. M. Koonen, "Reconfigurable beam system for non-line-of-sight free-space optical communication," *Light: Sci. Appl.*, vol. 8, no. 1, 2019, Art. no. 69.

[7] T. Koonen, K. Mekonnen, F. Huijskens, Z. Cao, and E. Tangdiongga, "Novel broadband OWC receiver with large aperture and wide field-of-view," in *Proc. Eur. Conf. Opt. Commun.*, 2020, pp. 1–4.

[8] T. Umezawa, A. Matsumoto, K. Akahane, S. Nakajima, and N. Yamamoto, "Large submillimeter high-speed photodetector for large aperture FSO receiver," *IEEE J. Sel. Topics Quantum Electron.*, vol. 28, no. 2, Mar./Apr. 2022, Art. no. 3801709.

[9] P. Brandl, R. Enne, T. Jukić, and H. Zimmermann, "OWC using a fully integrated optical receiver with large-diameter APD," *IEEE Photon. Technol. Lett.*, vol. 27, no. 5, pp. 482–485, Mar. 2015.

[10] I.-C. Lu, C.-H. Yeh, D.-Z. Hsu, and C.-W. Chow, "Utilization of 1-GHz VCSEL for 11.1-Gbps OFDM VLC Wireless Communication," *IEEE Photon. J.*, vol. 8, no. 3, Jun. 2016, Art. no. 7904106.

[11] W. Ali et al., "Design and assessment of a 2.5-Gb/s optical wireless transmission system for high energy physics," *IEEE Photon. J.*, vol. 9, no. 5, Oct. 2017, Art. no. 7907208.

[12] W. Ali et al., "10 Gbit/s OWC system for intra-data centers links," *IEEE Photon. Technol. Lett.*, vol. 31, no. 11, pp. 805–808, Jun. 2019.

[13] G. Cossu et al., "VCSEL-based 24 Gbit/s OWC board-to-board system," *IEEE Commun. Lett.*, vol. 23, no. 9, pp. 1564–1567, Sep. 2019.

[14] Z. Cao, Z. Wei, S. Zhang, K. Ma, H. Fu, and Y. Dong, "Misalignment analysis of a high-speed uplink OWC system based on a 940-nm VCSEL," *IEEE Photon. Technol. Lett.*, vol. 33, no. 18, pp. 1022–1025, Sep. 2021.

[15] Y. Song, C. Li, K. A. Mekonnen, E. Tangdiongga, M. Spiegelberg, and O. Raz, "Large aperture receiver based on co-packaged micro-lens and PD arrays for indoor GbE OWC links," in *Proc. Eur. Conf. Opt. Commun.*, 2022, pp. 1–4.

[16] S. Battiato, A. R. Bruna, G. Messina, and G. Puglisi, *Image Processing for Embedded Devices*. Sharjah, UAE: Bentham Science Publishers, 2010.

[17] E. Sarbazi, H. Kazemi, M. D. Soltani, M. Safari, and H. Haas, "Design tradeoffs of non-imaging angle diversity receivers for 6G optical wireless access networks," in *Proc. IEEE Glob. Commun. Conf.*, 2022, pp. 419–424.

[18] C. W. Oh, Z. Cao, E. Tangdiongga, and T. Koonen, "Free-space transmission with passive 2D beam steering for multi-gigabit-per-second per-beam indoor optical wireless networks," *Opt. Exp.*, vol. 24, no. 17, pp. 19211–19227, Aug. 2016.

[19] N. Q. Pham, K. A. Mekonnen, E. Tangdiongga, A. Mefleh, and A. M. J. Koonen, "Accurate indoor localization for beam-steered OWC system using optical camera," in *Proc. 45th Eur. Conf. Opt. Commun.*, 2019, pp. 1–4.

[20] M. Curran, K. Zheng, H. Gupta, and J. Longtin, "Handling rack vibrations in FSO-based data center architectures," in *Proc. Int. Conf. Opt. Netw. Des. Model.*, 2018, pp. 47–52.

[21] A. R. Ndjiongue, T. M. N. Ngatched, O. A. Dobre, A. G. Armada, and H. Haas, "Analysis of RIS-based terrestrial-FSO link over G-G turbulence with distance and jitter ratios," *J. Lightw. Technol.*, vol. 39, no. 21, pp. 6746–6758, Nov. 2021.

[22] T. Koonen, K. Mekonnen, F. Huijskens, N. Q. Pham, Z. Cao, and E. Tangdiongga, "Optical wireless GbE receiver with large field-of-view," in *Proc. Eur. Conf. Opt. Commun.*, 2021, pp. 1–4.

[23] M.-G. Han, Y.-J. Park, S.-H. Kim, B.-S. Yoo, and H.-H. Park, "Thermal and chemical stability of reflowed-photoresist microlenses," *J. Micromechanics Microengineering*, vol. 14, no. 3, 2003, Art. no. 398.

[24] C. Barbio, K. A. Mekonnen, F. Huijskens, T. Koonen, and E. Tangdiongga, "Bidirectional gigabits per second spatial diversity link using POF for passive optical front-ends," *J. Lightw. Technol.*, vol. 40, no. 20, pp. 6753–6761, Oct. 2022.

[25] A. Zaidi, F. Athley, J. Medbo, U. Gustavsson, G. Durisi, and X. Chen, *5G Physical Layer: Principles, Models and Technology Components*. Cambridge, MA, USA: Academic Press, 2018.